Renewable Energy 273 (2026) 126108

Contents lists available at ScienceDirect

Renewable Energy

journal homepage: www.elsevier.com/locate/renene

A field-scale model for simulating the redistribution of solar radiation and water on the ground surface under solar panels in agrivoltaic systems

Anh H. Nguyen [a], Yaoze Liu [a,*], Siyu Li [a], Zhuohang Wu [a], Majdi R. Abou Najm [b], Liming Zhou [c], Xiaobo Xue Romeiko [d], Richard R. Perez [e], Mark E. Uchanski [f], Jennifer M. Bousselot [f], Hu Liu [g], Chuandong Wu [h]

[a] Department of Environmental and Sustainable Engineering, University at Albany, State University of New York, Albany, NY, 12222, USA
[b] Department of Land, Air and Water Resources, University of California, Davis, CA, 95616, USA
[c] Department of Atmospheric and Environmental Sciences, University at Albany, State University of New York, Albany, NY, 12222, USA
[d] Department of Environmental Health Sciences, University at Albany, State University of New York, Rensselaer, NY, 12144, USA
[e] Atmospheric Sciences Research Center, University at Albany, State University of New York, Albany, NY, 12222, USA
[f] Department of Horticulture and Landscape Architecture, Colorado State University, Fort Collins, CO, 80523, USA
[g] Northwest Institute of Eco-Environment and Resources, Chinese Academy of Sciences, Lanzhou, 730000, China
[h] State Key Laboratory of Hydroscience and Engineering, Department of Hydraulic Engineering, Tsinghua University, Beijing, 100084, China

ARTICLE INFO

Keywords:
Solar photovoltaic panel
Solar radiation
Precipitation
Melted snow
Solar panel cleaning water

ABSTRACT

Agrivoltaic systems, which co-locate solar photovoltaic systems and croplands, can potentially optimize land use. However, current models cannot represent all key factors regarding solar radiation and water depth on the ground surface under solar panels. This study developed a field-scale model, AVS-Microclimate, that can represent the key factors focusing on redistributions of solar radiation, precipitation (rainfall and snowfall), melted snow (snow on panel and ground), and solar panel cleaning water on the ground surface under solar panels in agrivoltaic systems. The AVS-Microclimate model was demonstrated through three-dimensional simulations of an agrivoltaic site in Colorado, USA. The precipitation, melted snow, and solar panel cleaning water redistribution module were parameterized using observed data, which showed a strong alignment for water distribution (percent bias: −1.64%, coefficient of determination: 0.95, and Nash-Sutcliffe efficiency: 0.95). The redistribution of solar radiation and water depth (precipitation, melted snow, and solar panel cleaning water) on the ground grids varied greatly for different weather conditions, grids, and/or times (dates and times of a day). The AVS-Microclimate can assist decision-making by assessing how layouts (inclinations, azimuth angles, heights, spacing) and sizes (lengths/widths) of solar photovoltaic panels affect solar radiation and water depth under solar panels, which are critical for crop production in agrivoltaic systems.

1. Introduction

Global energy and food consumption is projected to increase significantly because of growing population and economic expansion [1]. These factors are driving research and development of renewable energy sources that can both complement and replace fossil fuels. In addition, the improvement of food production and increase of land use efficiency are essential to meet food security. Installing utility-scale photovoltaic (PV) solar arrays is one of the effective solutions to meet energy needs. In 2010, electricity from solar PV systems accounted for 4% of all new electricity-generating capacity additions in the United States, while the first three quarters of 2023 witnessed a rapid increase of this statistic to 48% [2]. However, building more solar PV systems requires large amounts of land. This has resulted in competition for land that has previously been utilized for agricultural purposes [3]. Furthermore, water use is crucial for irrigated agriculture. As water scarcity and depletion increase, its capacity to sustain agriculture is diminishing. Therefore, effective management of solar energy, food production, and water use in the context of Food-Energy-Water (FEW) nexus is a key challenge for sustainable development.

Agrivoltaic systems (AVS), which co-locate solar PV systems and cropland areas of agro-ecosystems to generate food and electricity, are

* Corresponding author.
E-mail address: yliu46@albany.edu (Y. Liu).

https://doi.org/10.1016/j.renene.2026.126108
Received 10 November 2025; Received in revised form 18 June 2026; Accepted 18 June 2026
Available online 19 June 2026

increasingly being recognized as a sustainable way to address the simultaneous issues of food security, water use, and renewable energy generation [4,5]. These systems, designed to exploit solar energy on agricultural land, provide a promising pathway towards maximizing land use efficiency and fostering symbiotic relationships between farming and energy production [6]. By mounting solar PV panels above crops, AVS not only generate clean electricity but also provide shade, which may lead to reduced water evaporation, improved plant growth conditions, and potentially increased agricultural yield in certain environments. This dual-use approach addresses the often competing demands for land by promoting coexistence and mutual benefit [7].

The microclimate, water, electricity generation, and crop growth in AVS have been investigated by field-scale experiments [3,8]. In addition, some computer models were developed to simulate AVS [9]. The impacts of AVS on electricity generation, crop growth/yield, and water quantity/quality in the context of Food-Energy-Water nexus are influenced by various key factors. These factors include the layouts (inclinations, azimuth angles, heights, spacing) and sizes (lengths/widths) of solar PV panels, solar panel efficiency (self-shading, solar panel temperature, dust coverage, and snow coverage), crop species, field scale microclimate under/near solar panels (precipitation, wind, air temperature, solar radiation, and relative humidity), soil types and properties (moisture, temperature, and chemicals), and water usage (solar panel cleaning and irrigation).

Although solar panels can alter air temperature, wind speed, and relative humidity under solar panels [6,8] and these can lead to the changes in soil moisture and evapotranspiration, the scope of the present study focuses on the redistributions of solar radiation, precipitation (rainfall and snowfall), melted snow (snow on panel and snow on ground), and solar panel cleaning water under solar panels in AVS. Processes such as evapotranspiration under solar panels, soil moisture dynamics, PV panel temperature, PV efficiency, solar panel self-shading, and atmospheric variables (air temperature, wind speed, and relative humidity under solar panels) are not explicitly modeled and are considered outside the scope of the present study. However, current computer models lack the ability to represent all key factors regarding the redistributions of solar radiation, precipitation (rainfall and snowfall), melted snow (snow on panel and snow on ground), and solar panel cleaning water on the ground surface under solar panels in AVS, which are critical components of microclimatic conditions affecting crop production.

For example, Amaducci et al. [10] created a radiation model to simulate solar radiation distribution in AVS that uses two-axis trackers. The "study area unit" was represented by a polygon divided into pixels. At each time step, the condition of a pixel (whether shaded or not) was established by overlapping the shaded region with the study area. Only diffuse radiation was received by shaded pixels, while unshaded pixels received both diffuse and direct radiation. However, the model cannot simulate water redistribution under solar panels. A tool was developed by Silva et al. [11] for calculating the reduced solar radiation on solar PV panels due to surrounding obstacles (e.g., buildings). However, the method in the tool needs to be improved to calculate the solar radiation reaching the ground under solar PV panels.

In addition, the three-dimensional (3D) redistribution of precipitation (rainfall and snowfall), melted snow (snow on panel and snow on ground), and cleaning water beneath solar panels has not been adequately considered in previous studies. Elamri et al. [12] developed the AVRAIN model to analyze rain distribution in a field-scale AVS as a function of solar PV panel tilt, height, and size; however, the model only includes the vertical (x, z) plane without evaluating the significant effects of wind on rainfall in the y direction. Therefore, an approach needs to be created to represent the redistribution of precipitation, melted snow, and cleaning water in 3D direction under solar panels. No previous studies considered the relationship between depression storage depth and tilt angle of solar PV panels, which is important for water balance in both non-tracking and tracking PV systems.

Therefore, a field-scale model capable of representing the key processes governing solar radiation and water redistribution beneath solar panels is needed to support decision-making in AVS design and management. The objectives of the paper were: (1) develop a field-scale model (AVS-Microclimate) focusing on the redistributions of solar radiation, precipitation (rainfall and snowfall), melted snow (snow on panel and snow on ground), and solar panel cleaning water under solar panels in AVS; and (2) demonstrate the AVS-Microclimate model to simulate the impacts of AVS on the redistribution of solar radiation and water depth (precipitation, melted snow, and solar panel cleaning water) under solar panels in a case study area.

This study contributes a novel field-scale model that simulates the redistribution of solar radiation and water (rainfall and snowfall, snowmelt on both panels and ground, and solar panel cleaning water) on the ground surface beneath solar panels in AVS. Unlike existing approaches, the model integrates these processes within a three-dimensional framework and enables assessment of how panel layout (inclination, azimuth angle, height, and spacing) and size influence spatial patterns of solar radiation and water depth beneath the panels. These capabilities can assist decision-making in AVS design, with direct relevance to crop production.

2. Creation of the AVS-Microclimate model to assess the redistributions of solar radiation, precipitation, melted snow, and solar panel cleaning water under solar panels in AVS

2.1. Ground and solar panel position module

The ground is created by four vertices (V_1, V_2, V_3, and V_4) using Cartesian coordinates (Fig. 1), and each vertex is displaced by executing two rotations and one translational movement (D) [11]. Specifically, each vertex's coordinate (with the coordinates of v_x, v_y, and v_z) is multiplied by rotation matrices (R_y and R_z) to carry out the two rotations. The first rotation occurs around the y-axis and is associated with the tilt angle (β) of the ground. The second rotation occurs around the z-axis and relates to the azimuth angle (γ) of the ground. The translational displacement is achieved by adding the displacement vector (D) to the coordinate of each vertex (Eq. (1) and Eq. (2)). More details are in the paper by Silva et al. [11].

$$V_i = R_y(\beta) \times R_z(\gamma) \times \begin{pmatrix} v_x \\ v_y \\ v_z \end{pmatrix} + D \quad \text{Eq. 1}$$

$$R_y(\beta) = \begin{bmatrix} \cos\beta & 0 & \sin\beta \\ 0 & 1 & 0 \\ -\sin\beta & 0 & \cos\beta \end{bmatrix}; \; R_z(\gamma) = \begin{bmatrix} \cos\gamma & -\sin\gamma & 0 \\ \sin\gamma & \cos\gamma & 0 \\ 0 & 0 & 1 \end{bmatrix} \quad \text{Eq. 2}$$

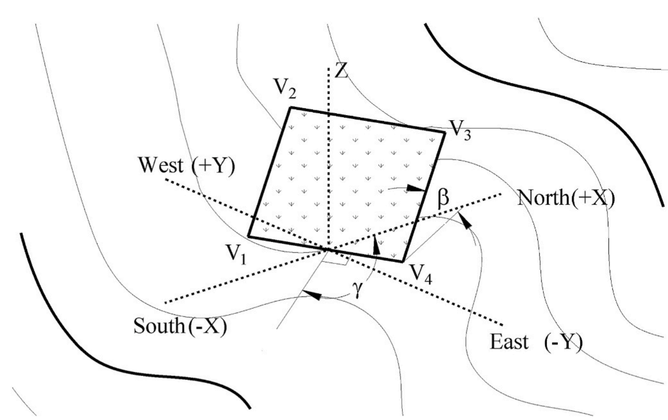

Fig. 1. The vertices of each ground corner with tilt angle (β) and azimuth angle (γ) [11].

Using the above method, the ground is divided into square grids to analyze the changes in each grid of the ground. Similar to the ground, a solar panel is represented by eight vertices. Each vertex represents one of the solar panel's corners using the dimensions of length, width, thickness, position, tilt angle, and azimuth [11].

2.2. Solar radiation redistribution module

2.2.1. Create the shading of solar panels on the ground

The shading of the direct radiation occurs if an object (i.e. a solar PV panel) is placed between the position of the sun and the ground. Sun position, expressed by the elevation angle (α_s) and azimuth (γ_s), is determined using the Sun Position Algorithm [13] (Fig. 2a).

Fig. 2b shows one projected vertex of the solar panel on the ground for each timestep. Vectors V_i (i = 1,2,3,4) are the corners of the ground while vectors P_i (i = 1,2,3,4) are used to determine four vertices of a solar panel. The coordinates of shadow projection (S_1) are calculated as the intersection of a ray (defined by the solar panel vertex P_1) and a plane (defined by the ground V_1,V_2,V_3, and V_4) [11,14] (Fig. 2b). The following equations (Eq. (3), Eq. (4), and Eq. (5)) determine the shadow position (S_1) of a single point P_1 between the sun and a surface [14].

$$S_1 = P_1 - \left[\frac{a \times (P_1 - V_1)}{a \times s}\right] \times s \qquad \text{Eq. 3}$$

$$a = (V_4 - V_1) \times (V_2 - V_1) \qquad \text{Eq. 4}$$

$$s = \begin{bmatrix} \cos\gamma_s.\cos\alpha_s \\ \sin\gamma_s.\cos\alpha_s \\ \sin\alpha_s \end{bmatrix} \qquad \text{Eq. 5}$$

where a is a vector perpendicular to the panel; P_1 is the vertex of a solar panel corner; S_1 is the projection of P_1 on the plane defined by the panel;

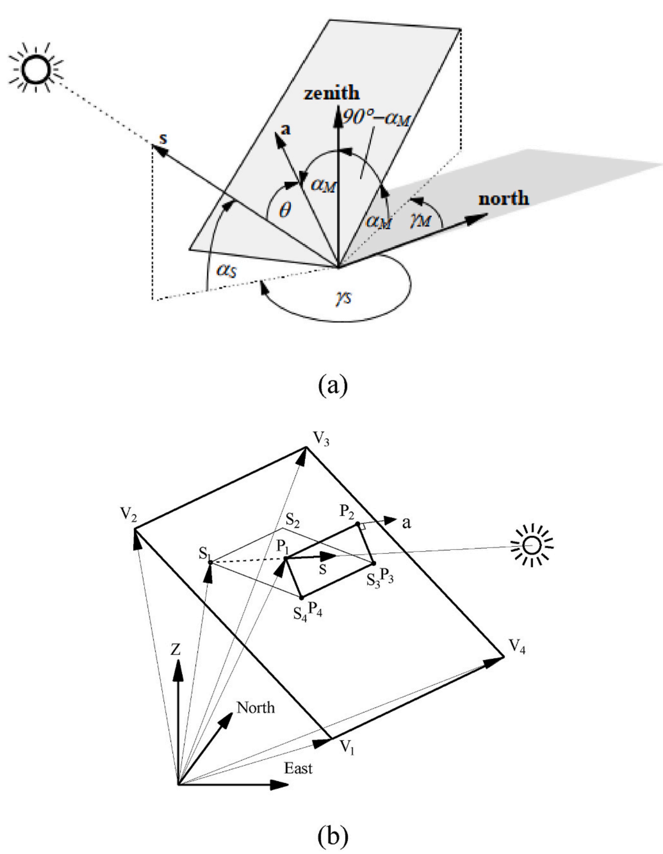

Fig. 2. Relationship between the angles at a tilted solar panel (a) and determination of the shadow position of a solar panel vertex (b) [14].

and s is the unit vector indicating the position of the sun. The other coordinates of shadow projection (S_2, S_3, and S_4) are calculated using the same approach. Further details about creating shadow on a tilted plane due to an object are in Quaschning and Hanitsch [14].

2.2.2. Calculate the solar radiation beneath solar panels

The shadows cast by solar PV panels on the ground vary in size and position as the sun moves. Shading factors, including direct shading factor (f_B) and diffuse shading factor (f_D) that lower the amount of light reaching the ground surface, is a common method to present the effect of shadows on a surface [14]. Solar radiation under solar panels is calculated for each grid using the following steps.

- Divide the ground into many square grids with specific sizes (e.g., 1m × 1m) to precisely compute the shaded area.
- Calculate the f_B and f_D for each grid at each timestep. A shading table is created as a matrix of direct shading factors [11]. The columns correspond to sun azimuth angles and the rows correspond to sun elevation angles. All azimuth angles from −180° to +180° and elevation angles from 0° to 90° are applied to compute the shading factors.
  (i) Direct shading factor (Eq. (6)).

$$f_B = \frac{A_{shade}}{A_{tot}} \qquad \text{Eq. 6}$$

where A_{shade} is the shaded area obtained by the projection on the ground (m^2); and A_{tot} is the total ground area (m^2).

(ii) Diffuse shading factor.

This factor is constant over time and has to be determined only once [11,14]. For an isotropic and discretized sky, the shading table was also used to estimate the diffuse shading factor in Eq. (7) [11].

$$f_D = \frac{\sum_{i=1}^{91}\sum_{i=1}^{361} f_{bij}\ \cos(\theta_{ij})\cos(\alpha_i)}{\sum_{i=1}^{91}\sum_{i=1}^{361}\cos(\theta_{ij})\cos(\alpha_i)} \qquad \text{Eq. 7}$$

where $\cos(\theta_{ij})$ is the angle of incidence at elevation angle i (from 0 to 90°) and azimuth j (from 0 to 360°); $\cos(\alpha)$ factor takes into account that the hemisphere subdivisions are smaller when the elevation angle is closer to 90° [11].

- Calculate direct and diffuse radiation (Eq. (8), Eq. (9)) reaching the grids [14]:

$$I_{t,s} = (1 - f_B) \times I_b \qquad \text{Eq. 8}$$

$$D_{t,s} = (1 - f_D) \times I_d \qquad \text{Eq. 9}$$

where $I_{t,s}$ is the direct radiation on a tilted and shaded plane (the grids); I_b is the direct radiation; and f_B is direct shading factor; $D_{t,s}$ is the diffuse radiation reaching the grids; I_d is the diffuse radiation; and f_D is the diffuse shading factor. I_b and I_d are calculated based on the methodologies described in previous studies [15,16].

- Calculate irradiance (Eq. (10)) reaching the grids ($G_{t,s}$) [14]:

$$G_{t,s} = I_{t,s} + D_{t,s} \qquad \text{Eq. 10}$$

This study focuses on the redistribution of solar radiation and water on the ground beneath solar panels. Surface albedo effects, which can influence radiation interactions, are beyond the scope of the present study and are therefore not explicitly considered.

2.3. Snowfall and snowmelt module

As part of the snow module of the AVS-Microclimate model, the snowfall and snowmelt module integrated the methods in the Soil and Water Assessment Tool (SWAT) [17]. If the mean daily air temperature is lower than the boundary temperature (T_{s-r}), precipitation is classified as snowfall, and the snow water equivalent (volume of water contained in the snowpack) is added to the snowpack. The snowpack at the ground surface will increase with further snowfall, or diminish through snowmelt or sublimation. The mass balance for the snowpack is calculated in Eq. (11):

$$SNO_t = SNO_{t-1} + R_{day,t} - E_{sub,t} - SNO_{mlt,t} \quad \text{Eq. 11}$$

where SNO_t and SNO_{t-1} are the water content of the snowpack on day t and day t−1, respectively (mm H_2O), $R_{day,t}$ is the amount of precipitation on day t (mm H_2O), $E_{sub,t}$ is the amount of sublimation on day t (mm H_2O), and $SNO_{mlt,t}$ is the amount of snowmelt on day t (mm H_2O).

The following equation (Eq. (12)) is used to compute the snowmelt on a given day.

$$SNO_{mlt,t} = b_{mlt} \times sno_{cov} \times \left[\frac{T_{snow} + T_{mx}}{2} - T_{mlt}\right] \quad \text{Eq. 12}$$

where $SNO_{mlt,t}$ is the amount of snowmelt on day t (mm H_2O), b_{mlt} is the melt factor (mm H_2O/day-^oC), sno_{cov} is the fraction of the area covered by snow, T_{snow} is the snow pack temperature (^oC), T_{mx} is the maximum air temperature (^oC), and T_{mlt} is the base temperature above which snowmelt is allowed (^oC). The calculation of other parameters is detailed in Neitsch et al. [17].

When there is snowpack on solar panels or ground, snowmelt occurs; and when the snowpack is no longer present, the melting stops. The melted snow from solar panels falls on the ground, while slid snowpack from solar panels [18] is added to the snowpack on the ground.

2.4. Precipitation, melted snow, and solar panel cleaning water redistribution module

The 3D redistribution of precipitation (rainfall/snowfall), melted snow, and cleaning water in the AVS-Microclimate model considers ground features, solar PV panel features, and wind velocity/direction. The following section outlines the steps following the same computational framework used for solar radiation, with necessary modifications to suit this context.

- Create ground and solar panel positions (shown in Section 2.1).
- Estimate shading area on the ground.

To model the shading area created by precipitation (i.e., area on the ground not receiving direct rainfall or snowfall due to solar panels), we developed a method analogous to that used for calculating shading from direct solar radiation. This approach is justified by the approximate geometric similarities in how both solar radiation and precipitation produce shadows (Table 1). Consequently, the rainfall/snowfall direction, rather than the solar radiation path, is employed to determine the "rain shade" or "snow shade" area on the ground. This direction is derived from the precipitation elevation angle (a function of wind and falling precipitation velocities) and the precipitation azimuth (which follows the wind direction) (Table 1, Eq. (13)).

The rainfall or snowfall direction follows the wind direction [12], as shown in Eq. (13):

$$\tan(\alpha_R) = \frac{V_w}{V_d} \quad \text{Eq. 13}$$

where α_R is the angle of incidence of precipitation with respect to the vertical axis; V_w is the velocity of the wind (m/s); and V_d is the velocity of the falling precipitation (m/s).

Table 1
Similarities in creating the shading of solar radiation and precipitation.

Comparison	Solar radiation	Precipitation (Rainfall or snowfall)
Shading on ground caused by solar panels	Shading created as described in section 2.2	"Rain shade" or "snow shade" results in no direct precipitation in the shaded area
Factor to determine shading	Direct radiation	Rainfall or snowfall
Position to be determined	Sun elevation angle (0-90°) Sun azimuth (0-360°)	Precipitation elevation angle: The angle of incidence of rainfall or snowfall caused by the wind. Elevation angle = 90° - α_R Precipitation azimuth: Direction of wind (0-360°) from weather stations.

- Identify "rain shade" or "snow shade" on the ground. The "rain shade" or "snow shade" on the ground is identified from corner points of a solar panel (Fig. 3a). Any area on ground within the rain or snow shade does not have direct rainfall or snowfall, while any area outside the rain or snow shade has direct rainfall or snowfall.

- Calculate direct shading factor of rainfall or snowfall (f_p). Only direct shading factor is used because rainfall or snowfall is completely blocked by solar panels (impervious surface).
- Direct rainfall or snowfall depth on the rain-shaded plane s (in this case, it is the ground) with the presence of solar panels during the timestep t ($P_{t,s}$ in mm) is calculated in Eq. 14

$$P_{t,s} = (1 - f_P) \times P_t \quad \text{Eq. 14}$$

where P_t is the rainfall or snowfall from weather stations during the timestep (mm).

- Determine the water depth for every grid.
  a) The amount of rainfall or snowfall intercepted by solar panels (ΔP_t in mm) during timestep t is calculated in Eq. (15):

$$\Delta P_t = P_t - P_{t,s} \quad \text{Eq. 15}$$

b) Calculate the water depth of melted snow on solar panels (Section 2.3) and record water depth used for solar panel cleaning during the timestep.

c) Estimate evaporation and retained water on solar panels during timestep t in the water balance.
The Penman Monteith method (Eq. (16)) provides a good estimation of reservoir open-water evaporation [19]. The method is used to estimate the evaporation on the solar panel.

$$E = \frac{0.408\Delta(R_n - G) + \gamma_c \frac{900}{T+273} u_2 (e_s - e_a)}{\Delta + \gamma_c(1 + 0.34u_2)} \quad \text{Eq. 16}$$

where E is surface evaporation rate (mm day^{-1}); R_n is net radiation (MJ m^{-2} day^{-1}); G is soil heat flux density (MJ m^{-2} day^{-1}); T is mean daily air temperature at 2 m height (°C); u_2 is wind speed at 2 m height (m s^{-1}); e_s is saturation vapour pressure (kPa); e_a is actual vapour pressure (kPa); (e_s - e_a) is saturation vapour pressure deficit (kPa); Δ is slope vapour pressure curve (kPa °C^{-1}); and γ_c is psychrometric constant (kPa °C^{-1}).

The Penman–Monteith equation is applied only to water retained on panel surfaces (affects the redistribution of water reaching the ground surface). Penman–Monteith equation is not applied to crop or soil evapotranspiration because simulating evapotranspiration processes for soil/crops is not within the scope of this study.

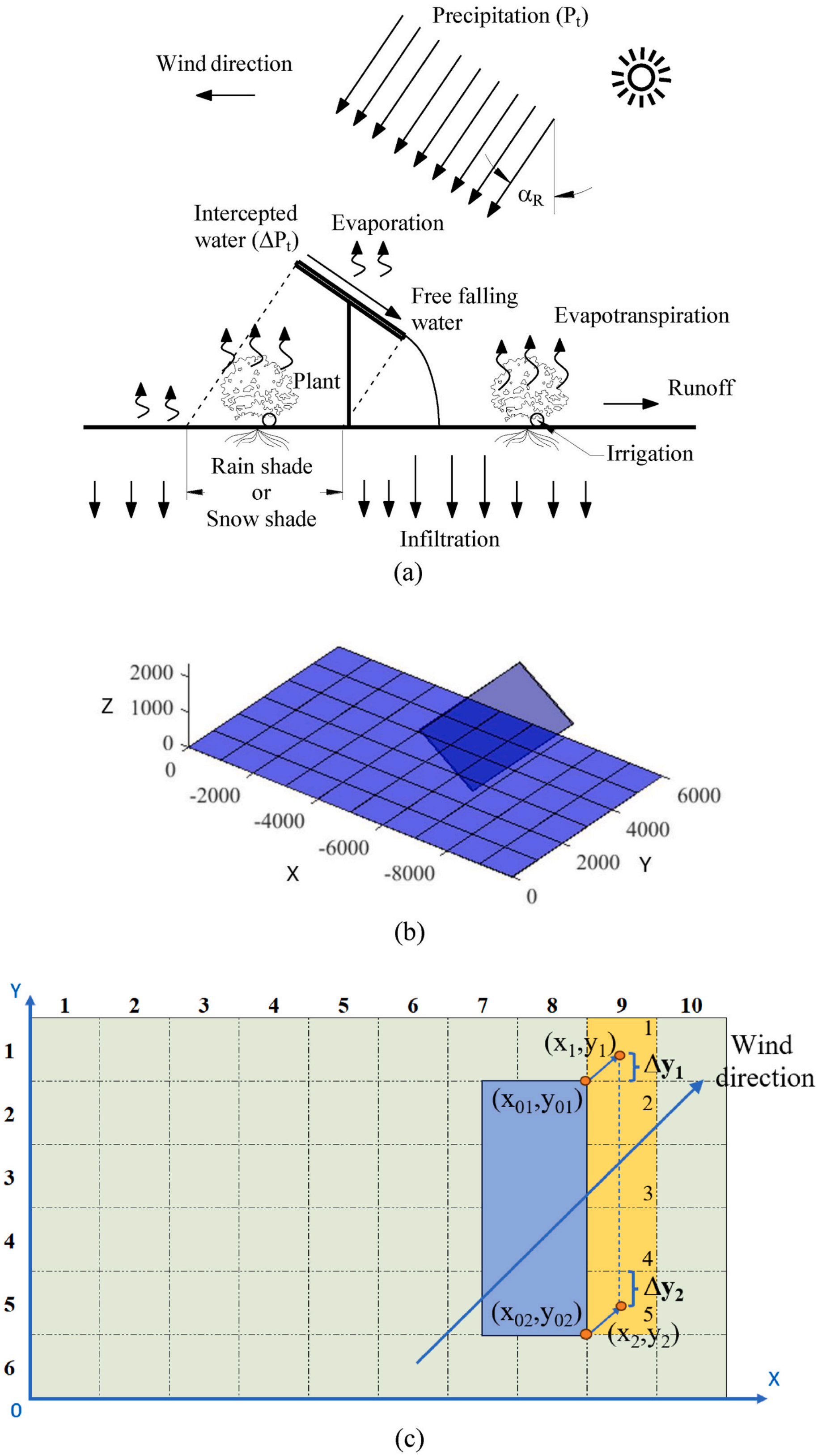

Fig. 3. (a) Water mass balance illustrating precipitation, rain shade and snow shade effects, and water-cycle processes in the AVS. (b) Three-dimensional representation of the study area used in the simulations; axis units are in millimeters (mm). (c) Top view of the study area showing the spatial distribution of free-falling water, where the yellow area indicates the free-fall zone. (For interpretation of the references to color in this figure legend, the reader is referred to the Web version of this article.)

Retained water (depression storage depth) on solar panels (ds), in Fig. 4, is calculated by revising the method in the Storm Water Management Model (SWMM) [20], as shown in Eq. (17):

$$\frac{\partial d}{\partial t} = P - E - q \quad \text{Eq. 17}$$

where P is the rate of rainfall, melted snow, or solar panel cleaning water intercepted on solar panels (mm/hour); E is the surface evaporation rate (mm/hour); d is the water depth accumulated above the panel surface during the timestep (mm); and q is the rate of free-falling water reaching the ground (water accumulated above ds) (mm/hour), presented in Fig. 3a.

The value of ds can be calculated by comparing the modeling results of free-falling water depth to experimental measurements. In addition, a method was created in the AVS-Microclimate model to calculate ds values for different tilt angles. For example, ds value is initially calculated to be 0.85 mm at a 50° tilt angle based on experimental data (Fig. S1a in supplementary material). To determine ds values for other tilt angles, a hypothetical triangle with sides a and b is constructed to store water at the panel's lower edge (Fig. S1b in supplementary material). The triangular area (A_{tr}) and rectangular area (A_{sq}) (Table S1 in supplementary material) are maintained equal. Using the known ds value of 0.85 mm and the 50° angle, the value of a is calculated. This value is then used to calculate b for different tilt angles (β). Subsequently, new triangular areas ($A_{tr,new}$) and rectangular areas ($A_{sq,new}$) are calculated (Table S1 in supplementary material). Finally, the corresponding new ds values for different tilt angles are determined.

d) Determine locations of free-falling water reaching grids.

After rainfall, snowfall (melted snow), and solar panel cleaning water are intercepted by solar panels and stored on solar panels, the remaining water becomes free-falling water from solar panels. Two points (x_{01}, y_{01}) and (x_{02}, y_{02}) are used to represent the lower edge of a solar PV panel (Fig. 3b and c). Two points (x_1, y_1) and (x_2, y_2), which represent the locations of free-falling water reaching grids, are determined using Eq. (18)–(23).

Water falling from the panels follows the parabolic trajectory. Runoff velocity is computed with the Manning-Strickler formula [12].

$$l_x = a_x \frac{T_x^2}{2} + V_x \cos \alpha_M T_x + x_o \quad \text{Eq. 18}$$

$$a_x = 2.10^{-4} \frac{(2.V_{wx}^2)}{D} \quad \text{Eq. 19}$$

$$T_x = \frac{V_x \sin \alpha_M + \sqrt{(V_x \sin \alpha_M)^2 + 2gz_o}}{g} \quad \text{Eq. 20}$$

where l_x is the location that the free-falling water reaches ground (m) in x direction; T_x is the free-falling duration (s) in x direction; α_M is the tilt angle of a solar panel (degree); a_x is the acceleration due to the wind in the x direction (m/s^2); V_{wx} is the wind velocity in x direction (m/s); V_x is the initial velocity of the free-falling water (m/s); D is diameter of a falling water drop (m); and x_o and z_o are the initial coordinates (m) of the falling water in the x and z direction of coordinate system, respectively.

To represent 3D processes, the (z-y) plane was created in the AVS-Microclimate model. The initial velocity of falling water in the direction of y (V_y) is assumed to be zero.

$$l_y = a_y \frac{T_y^2}{2} + V_y T_y + y_o \quad \text{Eq. 21}$$

$$a_y = 2.10^{-4} \frac{\left(2.V_{wy}^2\right)}{D} \quad \text{Eq. 22}$$

$$T_y = T_x \quad \text{Eq. 23}$$

where l_y is the location that the free-falling water reaches ground (m) in y direction; T_y is the free-falling duration (s) in y direction; a_y is the acceleration due to wind in the y direction; V_y is the initial velocity of the free-falling water (m/s); V_{wy} is the wind velocity in y direction; and y_o is the initial coordinate of falling water. The water drop is only affected by the wind.

After calculating the locations of free-falling water (x_1, y_1) and (x_2, y_2), the distribution line is determined (the dash line within yellow grids in Fig. 3c). The distribution of water depth on grids from free-falling water (Grids 1-5 in Fig. 3c) would be calculated proportionally using method in Table S2 (supplementary material). The water depth on the grid in this method will vary with grid size. Furthermore, the distribution line location will also be influenced by grid size and wind velocity. Distributed water depths are then added to the direct rainfall or snowfall (snowmelt) in each grid.

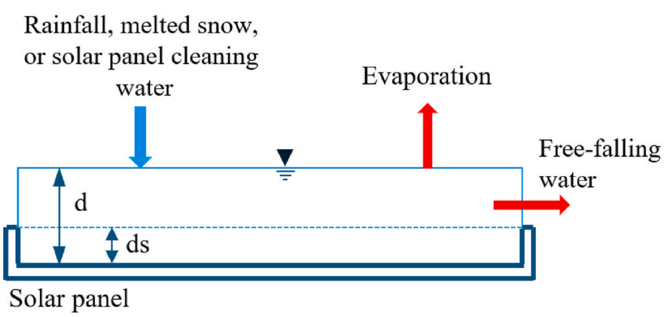

Fig. 4. Nonlinear reservoir model of a solar panel [20].

3. Case study: demonstration of the AVS-Microclimate model

3.1. Study area and data availability

The Agricultural Research, Development, and Education Center, South (ARDEC South), a part of Colorado State University (CSU), was selected as a case study area to demonstrate the application of the AVS-Microclimate model. Since 2018, CSU has been doing research in collaboration with Sandbox Solar of Fort Collins to experimentally investigate the impacts of small-scale pole-mounted solar PV panels on plants [21] (Fig. 5). Data in Table 2 from the experiment at ARDEC South and other sources were used to set up and demonstrate the AVS-Microclimate model. The dataset (2020–2022) originates from the most complete and reliable field observations available for the study site, and is therefore used in this current study. In addition, rain redistribution data (Table 3) were from Elamri et al. [12].

3.2. Case study demonstrating AVS-Microclimate model setup and components

The layout of the case study site at ARDEC South was set up in the

Fig. 5. AVS experiments at the ARDEC South adapted from Ref. [22].

Table 2
Data availability for the case study site at ARDEC South.

Type of data	Details
Data from the study at ARDEC South [22], [23]	
Location of the field	40.61° latitude and −104.99° longitude
Elevation of the field	1523 m
PV model	Jinko Solar's JKM325PP-72, 325W
PV material	Polycrystalline silicon (Opaque Si), 0% transparency
Size of solar panel	1956 mm × 992 mm × 41 mm
Operation inclination and facing	35°, face south
Height of the lower edge of PV array	1.22 m
Height of the upper edge of PV array	2.36 m
Size of area: Width × Length × Depth	60 m × 100 m × 1 m
Data from other sources	
Hourly precipitation from June 1, 2020 to September 30, 2022.	NASA Center for Climate Simulation [24]
Other hourly climate data (air temperature, relative humidity, solar radiation, and wind speed) from June 1, 2020 to September 30, 2022.	CoAgMET, Colorado State University [25]

Table 3
Rain redistribution data for parameterizing the precipitation, melted snow, and solar panel cleaning water redistribution module of the AVS-Microclimate model [12].

Type of data	Value
Tilt angle (α_{PV})	50°
Height of solar panel (above the ground)	5 m
Rainfall (P_0)	4.1 mm
Panel direction to the wind	Back to the wind
Size of a solar panel (width × length)	2 m × 1 m
Date	March 17th, 2016
Water depths in different locations (mm)	Varies

AVS-Microclimate model to simulate microclimate conditions under solar panels (Fig. 6). One PV array with four solar PV panels was simulated. The impacts of AVS on microclimatic conditions under solar panels were evaluated to demonstrate the AVS-Microclimate model.

- Calculate solar radiation redistribution on the ground co-located with solar PV panels in 3D space.
- The precipitation, melted snow, and solar panel cleaning water redistribution module of the AVS-Microclimate model was parameterized using the rain redistribution data (Table 3) in Elamri et al. [12] considering the relationship between depression storage depth and tilt angle of solar PV panels, which is important for water balance in both non-tracking and tracking PV systems. The size of ground grid (width × length) for simulation was 0.3 m × 0.3 m. As Elamri et al. [12] did not provide wind velocity information, a range of wind velocity values were applied to find the best ds value. Case number 05 was selected for this comparison, as it provided both simulated and experimental results of rain redistribution by solar panels.
- Calculate precipitation (rainfall and snowfall), melted snow (snow on panel and snow on ground), and solar panel cleaning water redistribution on the ground co-located with solar PV panels in 3D space. The simulated solar panel cleaning with pressurized water was conducted by presuming that cleaning is triggered once the soiling ratio - reflecting cumulative soiling losses - drops below a user-defined threshold of 0.97. The cleaning process involves pressurized water spraying onto the PV panels, applied at a rate equivalent to 2.1 mm of water over 0.5 min for each m^2 of panel surface [26].

4. Results and discussion

The AVS-Microclimate model was developed in MATLAB. The model code is available upon request from the corresponding author. For the case study presented, simulations were conducted on a personal computer [CPU: core i7, RAM: 32 GB, OS: Windows 10]. A typical field-scale 3D simulation in this study area (60 m^2) with grid size of 1 m × 1 m required approximately 15 min. Computational demand scales primarily with spatial resolution and domain size. Increasing grid resolution and domain size increases runtime and memory requirements proportionally. Parallel computing can be used to increase computational efficiency.

4.1. Solar radiation redistribution on the ground co-located with solar PV panels

The hourly simulation of solar radiation redistribution on the ground co-located with solar PV panels was run over the period from 0:00 on June 1, 2020 to 23:00 on September 30, 2022. Two examples of sun

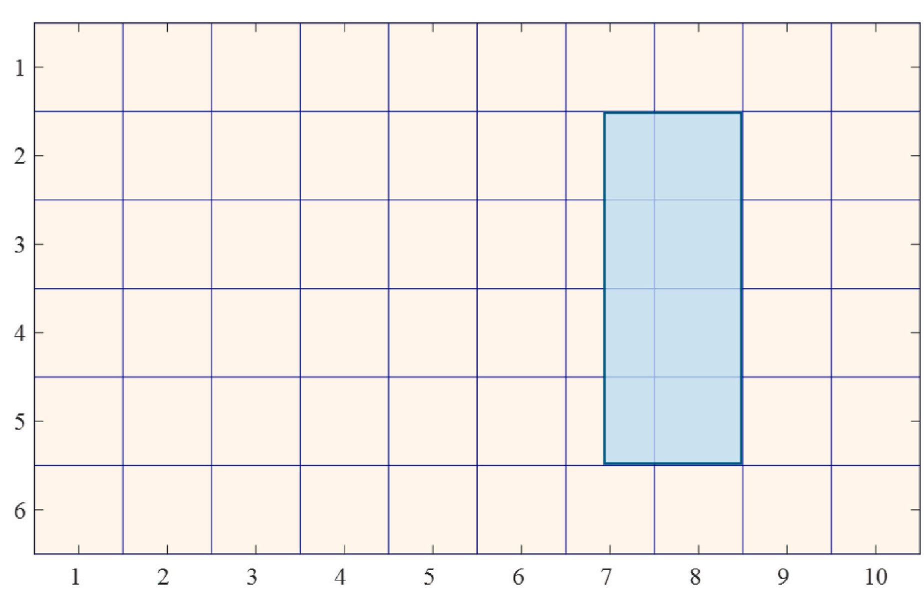

Fig. 6. Layout of the case study site at ARDEC South in the AVS-Microclimate model to simulate microclimatic conditions under solar panels (sizes of grids: 1 m × 1 m).

route in summer and winter were taken to show the results (Fig. S2 in supplementary material).

The first example happened in the summer at 12 p.m. on June 1, 2020, when the elevation angle of the sun reached the highest value of 80° and provided very strong solar radiation (798.6 Wh/m^2). The heatmap in Fig. 7a shows that the shaded grids beneath solar PV panels had significantly lower solar radiation compared to the grids far away from the panels. Two grids received the lowest solar radiation of 195.2 Wh/m^2.

For the second example happened in the winter at 12 p.m. on December 21, 2020, the sun elevation angle was at the lowest value of 30°. This led to significantly lower solar radiation (414.5 Wh/m^2) compared to the first example (Fig. 7b). One grid received the lowest solar radiation of 143.0 Wh/m^2. The shadow of solar PV panels in the winter was larger and further away from the solar panels compared to that in the summer. The results indicate that solar radiation redistribution on the ground grids co-located with solar PV panels vary for different grids and different times (dates and times of a day). During winter, lower solar elevation angles increase shadow length, resulting in deeper and more extensive low-radiation zones beneath the solar panel arrays compared to summer conditions. This pattern is consistent with findings reported by Appelbaum [27].

The results show that solar radiation at the most shaded grid reduced by up to 85% compared to the most exposed grid during summer. This finding is consistent with previous studies reporting substantial reductions in solar radiation beneath PV panels. For example, Wang et al. [28] reported an average reduction of approximately 75% between April and October, while another study has similarly observed significant shading effects beneath solar panel arrays [29]. The magnitude and spatial variability of solar radiation reduction depend on panel configuration, geographic location, and system design. In contrast to previous studies that reported averaged values, the present model provides high-resolution spatial representation of solar radiation redistribution across ground grids. This enables more detailed assessment of local solar radiation conditions and crop development beneath solar panels within AVS.

4.2. Parameterization of the precipitation, melted snow, and solar panel cleaning water redistribution module

By comparing the output of rainfall redistribution in the precipitation, melted snow, and solar panel cleaning water redistribution module of the AVS-Microclimate model with an experimental study in Elamri et al. [12], the ds value (depression storage depth on solar PV panels) was determined. Fig. S3 (supplementary material) illustrates the rain depths measured in twenty-one collectors which were expressed as grids. The grid 9 positioned beneath the lower edge of the panel received the largest amount of rainwater (8.4 mm), while grids farthest from the panel had a natural rainfall depth (4.1 mm) (Fig. S3 in supplementary material).

With the rainfall redistribution values from measured data (Table S4), water balance equation (Eq. (17)) was applied to calculate the ds value for each wind velocity. The values of ds increased with the decrease of wind velocity (Table S4). Compared to the results without considering ds (Table S3), the amount of rainwater on grid 9 was reduced so that the statistical indicators became much better for the wind speed from 0.4 to 0.8 m/s after considering ds (Table S5). For a wind speed of 0.4 m/s, the precipitation, melted snow, and solar panel cleaning water redistribution module demonstrated the best performance in simulating rainfall redistribution compared to both simulated and observed data in Elamri et al. [12], with percent bias (PBIAS) values of 5.37% and −1.64%, coefficient of determination (R^2) values of 0.93 and 0.95, and Nash–Sutcliffe efficiency (NSE) values of 0.86 and 0.95, respectively (Fig. 8). In accordance with the benchmarks set by Moriasi et al. [30], the obtained statistical indicators indicate very good model performance. Therefore, for the 50° tilt angle, the ds value of 0.85 mm was chosen for further simulation.

The corresponding ds value for each tilt angle was calculated. As in Fig. 9, the calculated ds values decreased with the increase of tilt angle. The ds values were interpolated to obtain the ds value of 35° tilt angle based on the ds values for tilt angles of 30° and 40°. Consequently, the ds value of 1.48 mm for 35° tilt angle was used to simulate the case study area at ARDEC South.

The parameter ds represents the depression storage depth used to calibrate water retention on the solar panel surface. Physically, this reflects the tendency of water to remain on panels when rainfall, snowmelt, or solar panel cleaning water occurs. Low panel inclination, surface micro-texture, and frame edges can reduce drainage efficiency, allowing thin water films or localized ponding to persist. These effects are further influenced by surface irregularities and partial blockage from dust or biofilm, as indicated in Powernsun [31]. Therefore, the calibrated ds parameter enables realistic representation of water retention on panel surfaces.

4.3. Precipitation, melted snow, and solar panel cleaning water redistribution on the ground co-located with solar PV panels

The redistribution of water depth on the ground co-located with solar PV panels due to precipitation (rainfall and snowfall), melted snow (snow on panel and snow on ground), and solar panel cleaning water was calculated over the simulation period.

On June 3, 2020 at 0:00 a.m. with natural rainfall of 0.12 mm/h, wind speed of 0.93 m/s, and wind direction azimuth of 80°, a heatmap of water depth distribution was created (Fig. 10). There was very little water (0 mm to 0.076 mm) on the grids fully or partially beneath the solar PV panel (from grid with the coordinate of row 2 and column 7 − 2×7 to grid of 5×8). Due to the wind direction, a grid right under the panel (grid 2×8) still received a rainfall depth of 0.034 mm, while other grids directly beneath the panel (3×8 to 5×8) remained dry. Four grids (yellow color) under the lower edge of panel received the largest amount of intercepted water at about 0.131−0.133 mm (from grid 2×9 to grid 5×9). Due to wind direction, grid 6×9 received less combined natural rainfall and intercepted water, resulting in a slightly lower water depth compared to natural rainfall. Water depths on grids 6×7 and 6×8 were lower than natural rainfall because the solar panel intercepted rainfall due to wind direction.

The results show substantial spatial variability in rainfall redistribution beneath the solar panels, with higher water accumulation near panel edges and lower water depth directly beneath central panel regions. This pattern is primarily caused by interception of rainfall by the panel surface and subsequent runoff toward panel edges, where water is concentrated and discharged onto the ground. Even under relatively low wind speeds, the direction of rainfall significantly influenced the location and magnitude of water accumulation on the ground surface. These findings indicate that water redistribution in AVS is not only controlled by panel shading but is also strongly affected by local meteorological conditions. Similar redistribution patterns have been observed in previous agrivoltaic studies, which reported localized increases in soil moisture near panel drip lines [12,32]. However, unlike previous studies that relied on 2D distribution, the present model provides detailed spatial representation of rainfall redistribution across ground grids. This enables improved understanding of heterogeneous water availability beneath solar panels, which is critical for optimizing crop placement and irrigation strategies in AVS.

Fig. 11 illustrates the water depth distribution on ground at 10 a.m. on December 17, 2020 due to snowmelt. The water depths due to snowmelt on the grids from 2×9 to 5×9 were the largest (approximately 0.069 mm) because these grids received all the snowmelt and snowpack falling from the solar panels. The water depths due to snowmelt on grids 2×7 to 5×8 (under the solar panels), which varied between 0.005 and 0.009 mm, were substantially lower compared to areas outside the solar panel coverage due to interception of snow by solar panels.

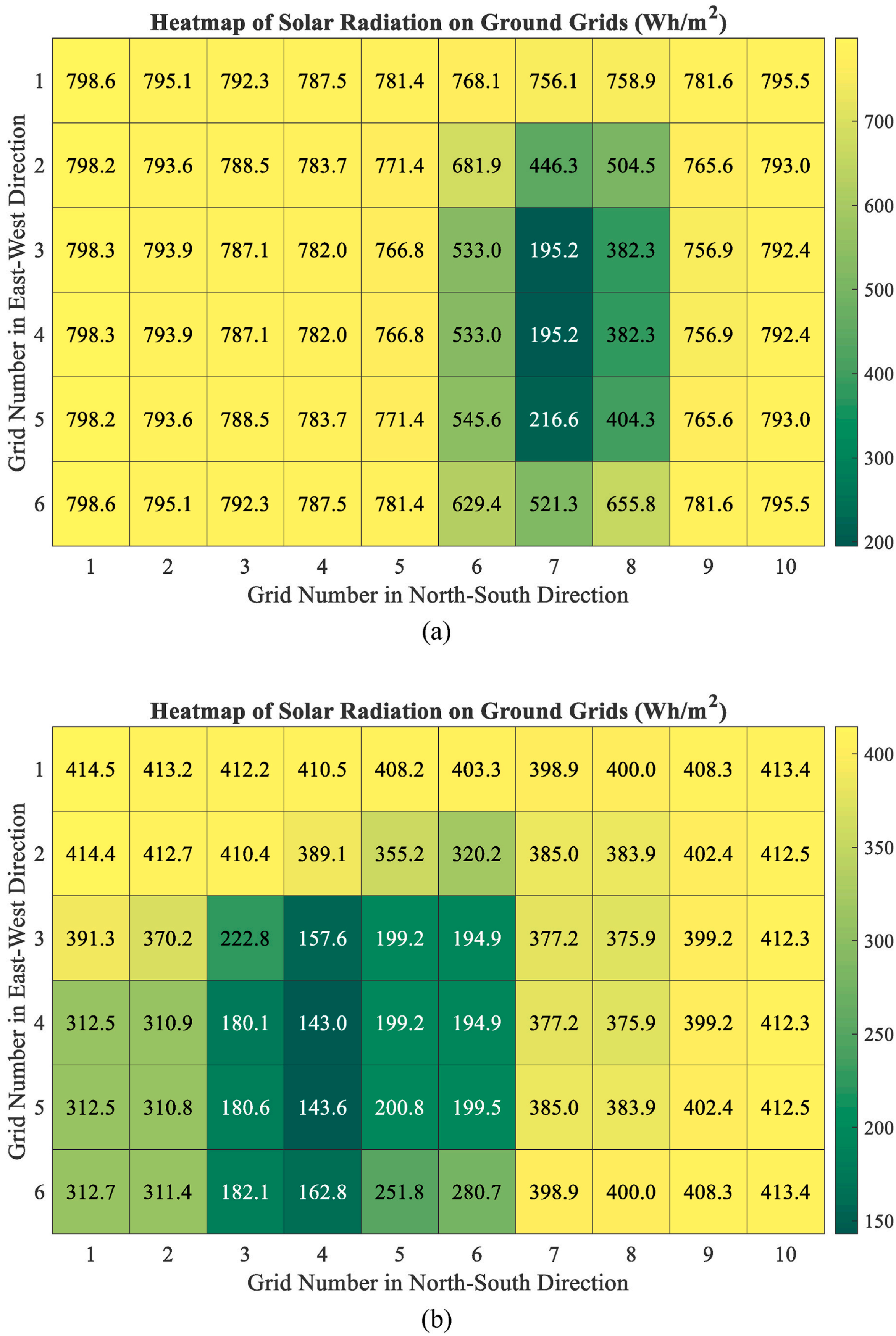

Fig. 7. Solar radiation redistribution in AVS at 12 p.m. on June 1, 2020 (a) and 12 p.m. on December 21, 2020 (b).

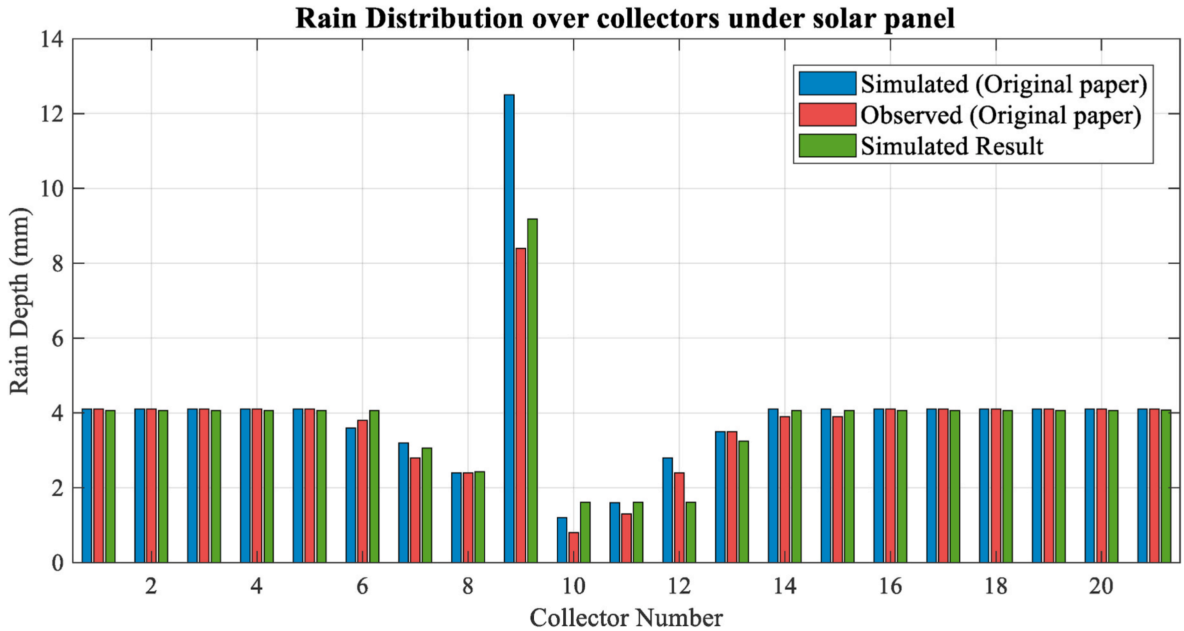

Fig. 8. Comparison of the observed and simulated results conducted by Elamri et al. [12] with the outputs of precipitation, melted snow, and solar panel cleaning water redistribution module.

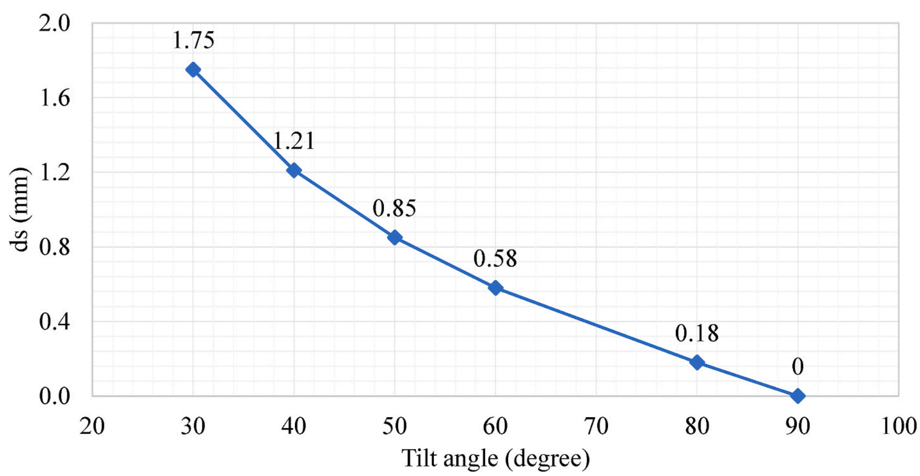

Fig. 9. The relationship between tilt angle and depression storage depth (ds) of solar PV panels.

The results demonstrate pronounced spatial variability in meltwater depth beneath the solar panels. Snow accumulation and melting behavior on PV panels differ from those on open ground due to panel tilt and surface properties. These factors influence snow retention and shedding processes, as indicated in previous studies [33,34]. These processes result in meltwater release and redistribution across ground surfaces, consistent with the spatial variability simulated in this study. The model's ability to capture this spatial redistribution provides improved insight into ground-level water availability during winter conditions and supports the evaluation of AVS design in cold climates. This detailed spatial quantification of snowmelt redistribution has not been explicitly represented in previous agrivoltaic modeling studies.

For the simulated event of solar panel cleaning with pressurized water, the water depth distribution on the ground at 10 p.m. on November 15, 2021 is presented in Fig. 12. It shows that the cleaning water from the solar panels was allocated onto grids from 1×9 to 5×9. The grids from 2×9 to 4×9 collected the greatest amount of water (about 0.110 mm) because they were directly under solar panel lower edges; while the grid 1×9 only received 0.0003 mm of water because it was on the side of the solar panels and wind blew water to the grid.

These results demonstrate that solar panel cleaning introduces localized water inputs rather than uniform redistribution across the ground surface. Such spatially uneven water distribution may influence soil moisture patterns and water availability beneath AVS, particularly in arid or semi-arid regions where cleaning events represent a significant water source. The model's ability to capture these detailed spatial redistribution patterns highlights its usefulness for evaluating hydrological impacts of solar panel maintenance and supporting optimized AVS design. This process has not been explicitly represented in previous agrivoltaic hydrological modeling studies. This spatial heterogeneity of the redistribution of solar panel cleaning water on the ground surface would affect soil moisture patterns and water availability, particularly in arid or semi-arid regions where solar panel cleaning water is an important hydrological source. By capturing these discrete patterns, the model effectively evaluates the impacts of solar panel maintenance on AVS design, a process overlooked in previous agrivoltaic modeling.

The observed heterogeneity in water distribution has important implications for crop growth and irrigation management. Localized

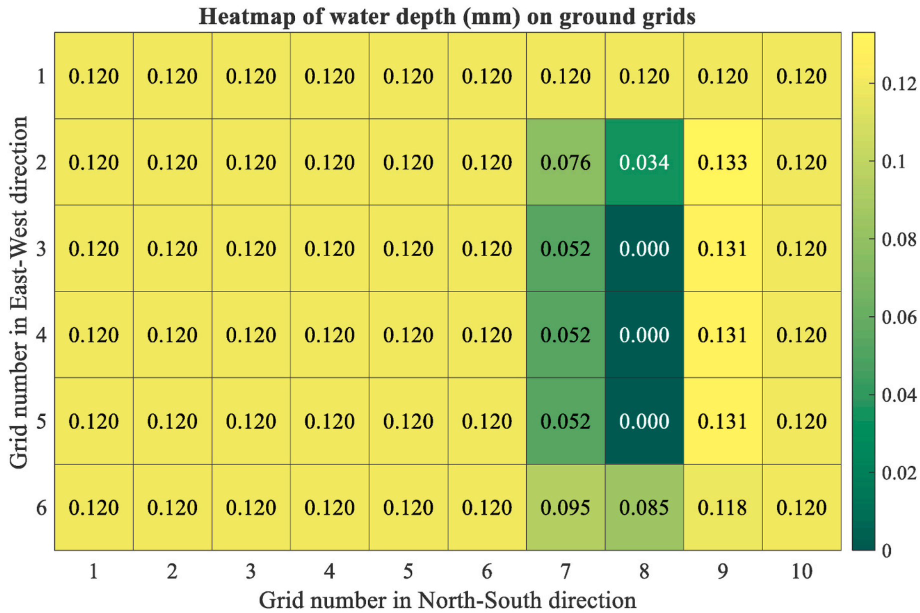

Fig. 10. Water depth distribution on grids at 0 a.m. on June 3, 2020 due to rainfall.

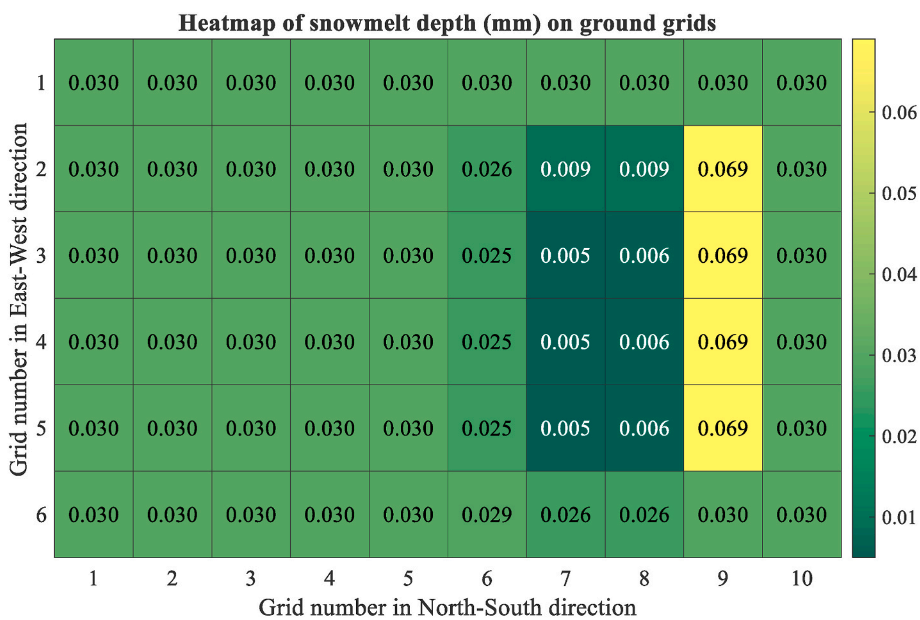

Fig. 11. Water depth distribution on ground at 10 a.m. on December 17, 2020 due to snowmelt.

zones of enhanced water availability near panel edges would reduce irrigation requirements and improve drought resilience, particularly in water-limited environments. Conversely, persistent spatial variability in soil water inputs could lead to uneven crop growth and yield if crop placement and irrigation scheduling are not adapted to these patterns. Therefore, understanding the spatial redistribution of water beneath PV panels is essential for optimizing agrivoltaic system design and maximizing both agricultural and energy production benefits.

5. Conclusions

This study developed a field-scale model (AVS-Microclimate) to simulate the redistributions of solar radiation and water (precipitation, snowmelt, and panel cleaning water) on the ground surface beneath solar panels in AVS. Application of the model in a three-dimensional space for an AVS in Colorado, USA demonstrated pronounced spatial variability in both solar radiation and water depth across ground grids beneath the panels. Solar radiation was substantially reduced beneath panel-covered areas, while water from rainfall, snowmelt, and panel cleaning were redistributed unevenly, with localized zones of higher and lower water accumulation depending on panel geometry, weather conditions, and spatial location, and/or time. These results highlight the strong influence of solar panel configuration on ground-level microenvironmental conditions. The AVS-Microclimate can assist decision-making by assessing the impacts of different layouts (inclinations, azimuth angles, heights, spacing) and sizes (lengths/widths) of solar PV panels on solar radiation and water depth under solar panels, which are critical for crop production in AVS.

Because of data constraints, only limited experimental observation was used to demonstrate the model. Future experiments can collect

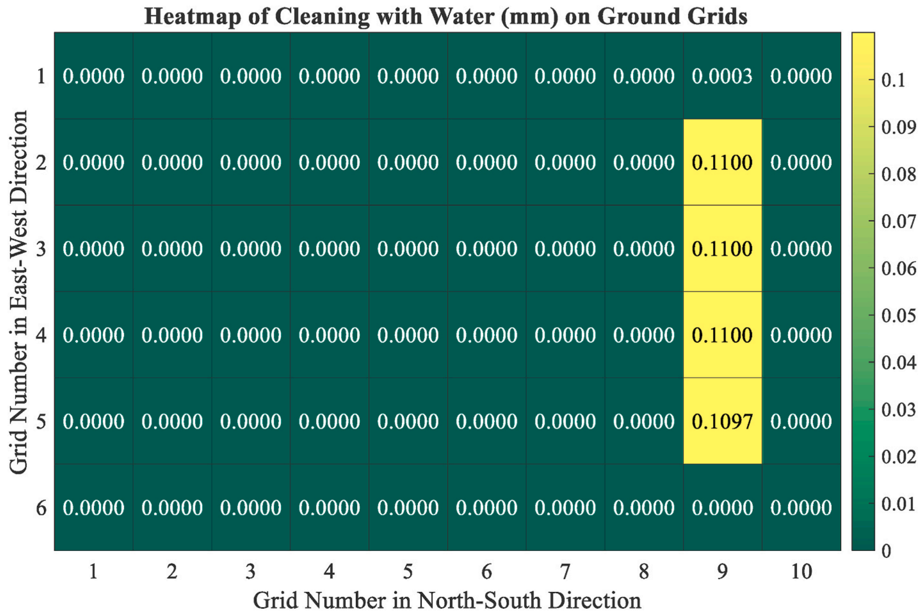

Fig. 12. Water depth distribution on ground at 10 p.m. on November 15, 2021 due to cleaning solar panels with water.

additional data on microclimatic conditions beneath solar panels and solar panel temperature, which will support (1) further calibration and validation of the AVS-Microclimate model; (2) adding the impacts of AVS on air temperature, wind speed, and relative humidity under solar panels to the AVS-Microclimate model; and (3) simulating the impacts of AVS (e.g., albedo and ambient temperature) on evapotranspiration under solar panels, crop growth/yield, solar panel temperature, and PV efficiency. In addition, uncertainty in the model results of this study arises from input data uncertainty, parameter uncertainty, and model structural uncertainty. In this study, uncertainty was not quantified explicitly due to the focus on process representation. In the future, uncertainty analyses should be conducted. Comparisons with commercial software can also be conducted in the future to further demonstrate the applicability of the model.

CRediT authorship contribution statement

Anh H. Nguyen: Formal analysis, Investigation, Methodology, Software, Validation, Visualization, Writing – original draft. **Yaoze Liu:** Conceptualization, Funding acquisition, Investigation, Methodology, Project administration, Resources, Software, Supervision, Writing – review & editing. **Siyu Li:** Formal analysis, Software, Writing – review & editing. **Zhuohang Wu:** Formal analysis, Software, Writing – review & editing. **Majdi R. Abou Najm:** Methodology, Writing – review & editing. **Liming Zhou:** Methodology, Writing – review & editing. **Xiaobo Xue Romeiko:** Methodology, Writing – review & editing. **Richard R. Perez:** Methodology, Writing – review & editing. **Mark E. Uchanski:** Methodology, Writing – review & editing. **Jennifer M. Bousselot:** Methodology, Writing – review & editing. **Hu Liu:** Methodology, Writing – review & editing. **Chuandong Wu:** Methodology, Writing – review & editing.

Declaration of competing interest

The authors declare that they have no known competing financial interests or personal relationships that could have appeared to influence the work reported in this paper.

Appendix A. Supplementary data

Supplementary data to this article can be found online at https://doi.org/10.1016/j.renene.2026.126108.

References

[1] A. Nguyen, T. Cochrane, M. Pahlow, Optimising water allocation and land management to mitigate the effects of land use and climate change on reservoir performance, Hydrol. Sci. J. 67 (14) (2022) 2129–2146.
[2] Solar Energy Industries Association, Solar Market Insight Report, 2023.
[3] H.A. Al-agele, K. Proctor, G. Murthy, C. Higgins, A case study of tomato (solanum lycopersicon var. legend) production and water productivity in Agrivoltaic Systems, Sustainability 13 (5) (2021) 2850, 1-13.
[4] G.A. Barron-Gafford, M.A. Pavao-Zuckerman, R.L. Minor, L.F. Sutter, I. Barnett-Moreno, D.T. Blackett, M. Thompson, K. Dimond, A.K. Gerlak, G.P. Nabhan, J. E. Macknick, Agrivoltaics provide mutual benefits across the food–energy–water nexus in drylands, Nat. Sustain. 2 (9) (2019) 848–855.
[5] J. Montes-Romero, A. Cruz-Escabias, F. Almonacid, E.F. Fernández, Comparative analysis of semi-transparent photovoltaic technologies for agrivoltaic applications, Renew. Energy (2025) 124573.
[6] G.A. Barron-Gafford, M.A. Pavao-Zuckerman, R.L. Minor, L.F. Sutter, I. Barnett-Moreno, D.T. Blackett, M. Thompson, K. Dimond, A.K. Gerlak, G.P. Nabhan, Agrivoltaics provide mutual benefits across the food–energy–water nexus in drylands, Nat. Sustain. 2 (9) (2019) 848–855.
[7] H. Dinesh, J.M. Pearce, The potential of agrivoltaic systems, Renew. Sustain. Energy Rev. 54 (2016) 299–308.
[8] E. Hassanpour Adeh, J.S. Selker, C.W. Higgins, Remarkable agrivoltaic influence on soil moisture, micrometeorology and water-use efficiency, PLoS One 13 (11) (2018) e0203256.
[9] S. Zainali, S. Ma Lu, B. Stridh, A. Avelin, S. Amaducci, M. Colauzzi, P.E. Campana, Direct and diffuse shading factors modelling for the most representative agrivoltaic system layouts, Appl. Energy 339 (2023) 120981.
[10] S. Amaducci, X. Yin, M. Colauzzi, Agrivoltaic systems to optimise land use for electric energy production, Appl. Energy 220 (2018) 545–561.
[11] M. Silva, J.J. Roberts, P.O. Prado, Calculation of the shading factors for solar modules with MATLAB, Energies 14 (15) (2021) 4713, 1-23.
[12] Y. Elamri, B. Cheviron, A. Mange, C. Dejean, F. Liron, G. Belaud, Rain concentration and sheltering effect of solar panels on cultivated plots, Hydrol. Earth Syst. Sci. 22 (2) (2018) 1285–1298.
[13] I. Reda, A. Andreas, Solar position algorithm for solar radiation applications, Sol. Energy 76 (5) (2004) 577–589.
[14] V. Quaschning, R. Hanitsch, Shade Calculations in Photovoltaic Systems, 1995. Citeseer.
[15] R. Perez, P. Ineichen, R. Seals, J. Michalsky, R. Stewart, Modeling daylight availability and irradiance components from direct and global irradiance, Sol. Energy 44 (5) (1990) 271–289.
[16] N.Z. Al-Rawahi, Y.H. Zurigat, N.A. Al-Azri, Prediction of hourly solar radiation on horizontal and inclined surfaces for Muscat/Oman, The Journal of Engineering Research [TJER] 8 (2) (2011) 19–31.
[17] S.L. Neitsch, J.R. Williams, J.G. Arnold, J.R. Kiniry, Soil and Water Assessment Tool Theoretical Documentation—Version 2009, Texas Water Resources Institute, College Station, 2011.

[18] B. Marion, R. Schaefer, H. Caine, G. Sanchez, Measured and modeled photovoltaic system energy losses from snow for Colorado and Wisconsin locations, Sol. Energy 97 (2013) 112–121.
[19] I.P. Craig, Comparison of precise water depth measurements on agricultural storages with open water evaporation estimates, Agric. Water Manag. 85 (1) (2006) 193–200.
[20] L.A. Rossman, Storm Water Management Model User's Manual Version 5.2, Version, 2022.
[21] Colorado Agrivoltaic Learning Center, Agrivoltaics 101. https://www.coagrivoltaic.org/agrivoltaics-101, 2018. (Accessed 7 July 2024).
[22] T. Hickey, Plant Growth Under Photovoltaic Arrays of Varying Transparencies–A Study of Plant Response to Light and Shadow in Agrivoltaic Systems, 2023.
[23] M. Uchanski, T. Hickey, J. Bousselot, K.L. Barth, Characterization of agrivoltaic crop environment conditions using opaque and thin-film semi-transparent modules, Energies 16 (7) (2023) 3012, 1-11.
[24] NASA, NASA Center for Climate Simulation Hourly Precipitation Data, 2024.
[25] CoAgMET, Colorado Agricultural Meteorological Network (Coagmet), 2024. https://coagmet.colostate.edu. (Accessed 1 February 2024).
[26] J. Qi, Q. Dong, Y. Song, X. Zhao, L. Shi, Combining dust scaling behaviors of PV panels and water cleaning methods, Renew. Sustain. Energy Rev. 212 (2025) 115394.
[27] J. Appelbaum, Shading and masking affect the performance of photovoltaic systems—a review, AIMS Energy 7 (1) (2019) 77–87.
[28] D. Wang, Y. Sun, Y. Lin, Y. Gao, Analysis of light environment under solar panels and crop layout, in: 2017 IEEE 44th Photovoltaic Specialist Conference (PVSC), 2017, pp. 2048–2053.
[29] Y. He, C.L. Tan, Y. Lu, Y. Qu, J. Liu, Solar radiation and daily light integral characteristics of photovoltaic-green roof system in tropical area: a case study in Singapore, Sol. Energy 279 (2024) 112807.
[30] D.N. Moriasi, M.W. Gitau, N. Pai, P. Daggupati, Hydrologic and water quality models: performance measures and evaluation criteria, Trans. ASABE 58 (6) (2015) 1763–1785.
[31] Powernsun, Do solar panels work in rain?. https://powernsun.com/do-solar-panels-work-in-rain/, 2026.
[32] C. Wu, H. Liu, Y. Yu, W. Zhao, J. Liu, H. Yu, O. Yetemen, Ecohydrological effects of photovoltaic solar farms on soil microclimates and moisture regimes in arid Northwest China: a modeling study, Sci. Total Environ. 802 (2022) 149946.
[33] E. Andenæs, B.P. Jelle, K. Ramlo, T. Kolås, J. Selj, S.E. Foss, The influence of snow and ice coverage on the energy generation from photovoltaic solar cells, Sol. Energy 159 (2018) 318–328.
[34] X. Huang, W. Gao, Y. Zhu, S. Yang, Study on the Natural Melting Time of Snow on Photovoltaic Modules, Workshop on Atmospheric Icing of Structures, 2022, pp. 1–6.